Nguyen, T. P., Wilczewski, S., Lewandowski, J., Majkowska-Pilip, A., Żelechowska-Matysiak, K., Nieciecka, D., Studziński, W., Olusegun, S. J., Syczewski, M. D., Giersig, M., Dinh, T. M. T., Krysiński, P., Osial, M. (2023): 5-fluorouracil and curcuminoids extract from Curcuma longa L. loaded into nanohydroxyapatite as a drug delivery carrier for SKOV-3 and HepG2 cancer cells treatment. - Ceramics International, 49, 15, 25775-25787.

https://doi.org/10.1016/j.ceramint.2023.05.123

5-fluorouracil and curcuminoids extract from *Curcuma longa* L. loaded into nanohydroxyapatite as a drug delivery carrier for SCOV-3 and HepG2 cancer cells treatment

Thu Phuong Nguyen[1]*, Sławomir Wilczewski[2,3], Jakub Lewandowski4, Agnieszka Majkowska-Pilip[5], Kinga Żelechowska-Matysiak[5], Dorota Nieciecka[6], Waldemar Studziński[2], Sunday Joseph Olusegun[6], Marcin Syczewski[7,8], Michael Giersig[3], Thi Mai Thanh Dinh[9], Paweł Krysiński[6] , Magdalena Osial[3]*

1 - Institute for Tropical Technology, Vietnam Academy of Science and Technology, 18 Hoang Quoc Viet, Cau Giay, Hanoi, Vietnam; nguyen-hong.nam@usth.edu.vn
2 - Bydgoszcz University of Science and Technology, Faculty of Chemical Technology and Engineering, Seminaryjna 3, 85-326 Bydgoszcz, Poland. email: slawomir.wilczewski@pbs.edu.pl
3 - Institute of the Fundamental Technological Research, Polish Academy of Sciences, Pawińskiego 45B Str., 02-106 Warsaw, Poland, e-mail: mgiersig@ippt.pan.pl, mosial@ippt.pan.pl
4 - Faculty of Physics, University of Warsaw, Pasteura 5 Str., 02-093 Warsaw, Poland, e-mail: j.lewandows2@student.uw.edu.pl
5 - Centre of Radiochemistry and Nuclear Chemistry, Institute of Nuclear Chemistry and Technology, Dorodna 16 Str., 03-195 Warsaw, Poland, e-mail: a.majkowska@ichtj.waw.pl, k.zelechowska@ichtj.waw.pl
6 - Faculty of Chemistry, University of Warsaw, Pasteura 1, 02-093 Warsaw, e-mail: dnieciecka@chem.uw.edu.pl, o.sunday@chem.uw.edu.pl, pakrys@chem.uw.edu.pl
7 - Faculty of Geology, University of Warsaw, Żwirki i Wigury 93, PL-02089 Warsaw, Poland, e-mail: m.d.syczewski@gmail.com
8 - Helmholtz Centre Potsdam - GFZ German Research Centre for Geosciences, Telegrafenberg, 14471 Potsdam, Germany
9 - University of Science and Technology of Hanoi, Vietnam Academy of Science and Technology, 18 Hoang Quoc Viet, Cau Giay, Hanoi, Vietnam; dinh-thi.mai.thanh@usth.edu.vn

Abstract
In this work, nanostructural hydroxyapatite (HAp) with a defined shape and size was prepared within the co-precipitation technique as a porous platform for the immobilization and release of an anticancer drug – 5-fluorouracil. The HAp was stabilized with the biologically active compounds extracted from Curcuma longa L. rhizome rich in curcuminoids like curcumin (curcumin I), demethoxycurcumin (curcumin II), bisdemethoxycurcumin (curcumin III), and cyclocurcumin. Morphological studies confirmed uniform rod-like shape sized in 8±1 nm diameter and 45±9 nm length. Due to the high surface:volume ratio HAp offered a high intake of biologically active compounds. Turbidimetry results confirmed the stability of the suspension in an aqueous media., and then, the interaction between the proposed nanocomposite and biomimetic membranes was studied revealing the effect on model membranes depending on the type of lipids. *In vitro* tests on SKOV-3 and HepG2 cell examined by MTS assay lines confirmed revealed the synergetic effect of the nanocomposite loaded

with drug and curcuminoids.

keywords: drug delivery, hydroxyapatite, curcumin extract, 5-fluorouracil, curcuminoids

1. Introduction

Cancer is a plague of the 21st century and without novel solutions or early diagnostics and treatment, the battle against it might be lost. For this reason, fast development of nanotechnology brings hope in cancer's treatment. One of the solutions is based on the application of the biocompatible nanomaterials that can release anticancer drug to the affected cells, and heal the tissues (Naahidi et al., 2013). They can maximize the pharmaceutical action of drugs was released by reducing the toxic side effects (Ranjha et al., 2022). Among many nanostructural materials, ~~the~~ hydroxyapatite nanoparticles reveal chemical and structural similarities with the natural bone tissues, resulting in biocompatibility (Zhou and Lee, 2011). It has gained attention in recent years, especially in ~~the~~ bone diseases diagnosis and therapeutics delivery (Ram Prasad et al., 2019). Due to its high surface-to-volume ratio and chemical composition, it promotes chemical and physical modifications making it an ideal platform for anticancer drug loading (Song et al., 2022). As a drug carrier, it can interact with biological cells resulting in multiple potentialities to be explored such as apoptosis induction to cancerous cells, cellular proliferation, angiogenesis, or tissue recovery (Ferreira-Ermita et al., 2020). In addition, it can promote cell adhesion and uptake. Hydroxyapatite (HAp) is a promising material in ~~the~~ drug delivery for its facile biocompatibility and facile functionalization to create the stable colloidal suspension (), (), (). HAp and its composites became noteworthy choices as drug carriers in bone regeneration treatment (Lee et al., 2021), (). The composites based on the HAp are also proposed as an anticancer platform for anticancer cancer treatment (Sun et al., 2018), (). It has also been recently tested in the ~~ran~~domized clinical trials offering high effectiveness in bone regeneration for its biocompatibility (Grocholewicz et al., 2020).

Curcuma longa L., also called turmeric is widely used as spice or food additive. It is also well known in a traditional medicine in Asia (Pan et al., 2020). This plant contain many valuable chemical compounds revealing biological activity, where the main active compounds are curcuminoids including curcumin I (known as curcumin), curcumin II (known as demethoxycurcumin), and curcumin III (known as bisdemethoxycurcumin), monoterpenoids, and sesquiterpenoids (Degot et al., 2021; Hadi et al., 2018). For the rich curcuminoids content, the turmeric extract is widely referred with literature for anti-inflammatory, anti-oxidativeand, and anti-cancer activity (Akter et al., 2019; Nurjanah and Saepudina, 2020). *Curcuma longa L.* offers promising anticancer effectiveness against different cancer types with very low or negligible toxicity to healthy cells. It is also presented it has curcuminoids reveal alleviating and suppressing the generation, transformation, proliferation, and metastasis of many different types of cancer cells (Khan et al., 2018). Additionally nanoparticle-mediated delivery of curcumin can improve the pharmacokinetic profile of medicines raising the chemotherapeutic potential (Mukerjee and Vishwanatha, 2009). Curcuminoids bring a lot of attention

Commented [p1]: https://wires.onlinelibrary.wiley.com/doi/full/10.1002/wnan.1504?casa_token=laBL3rKDdvMAAAAA%3AB-sqpvYNTvReNrrnAoVakT9dn8X1SnHVjp25bIDk3ByRfPRDA0QfFZGyi-c6cm_nQlAya4HsG2C8h3k

https://doi.org/10.1002/wnan.1504

Commented [p2]: https://link.springer.com/chapter/10.1007/978-3-030-10834-2_4

Commented [p3]: https://www.sciencedirect.com/science/article/pii/S0001868617300957?casa_token=sCmbr6RoDZAAAAAA:z7wfI_UJqg3bLX_tu8P_qtlq2WFCwkHNn8g_-ITK7XxnDHIwpLeD99MQ6uMFTI5x5GOQaNdYEA8

Commented [p4]: https://onlinelibrary.wiley.com/doi/full/10.1002/app.51893?casa_token=9y10hDWuQZEAAAAA%3AZ9md3_cPD_WLdvGb65j0dclLp8PBKQrCiYvXy2OnnFPLaFkraUP24e0G9gaQySAfVkcrJRcLj91fHZU

Commented [p5]: https://ceramics.onlinelibrary.wiley.com/doi/full/10.1111/ijac.13231?casa_token=K-ofaEHYZ20AAAAA%3AZiehCceQ2c27IEFLntPCYfnhHS1eZ29VxBjHmw4d-O7E-fX1afRxS2D8nYZMzE0-Yrm8mEHcRBKFHwg

in anticancer research for their biological activity. For example, turmerones being active ingredients in turmeric oil, has mainly anti-cancer property (). Therefore, both curcuminoids and other components of *Curcuma longa* L. rhizome account for the pharmacological efficacy of turmeric (Chao et al., 2018).

Commented [p6]: San, H.H.M.; Alcantara, K.P.; Bulatao, B.P.I.; Chaichompoo, W.; Nalinratana, N.; Suksamrarn, A.; Vajragupta, O.; Rojsitthisak, P.; Rojsitthisak, P. Development of Turmeric Oil—Loaded Chitosan/Alginate Nanocapsules for Cytotoxicity Enhancement against Breast Cancer. *Polymers* **2022**, *14*, 1835. https://doi.org/10.3390/polym14091835

In this work, the curcumin extract obtained from the *Curcuma longa* L. rhizome was proposed as a source of the biologically active components with high-efficiency and low-costs of preparation offering more active ingredients than the commercial curcumine-based powder. High Pressure Liquid Chromatography (HPLC) and gas chromatography (GC) confirmed the presence of nine biologically active compounds in the turmeric extract. It was used as a stabilizer of nanostructural hydroxyapatite prepared within the co-precipitation technique to prepare stable colloidal suspension as well as the agent working synergistically with anticancer drug - 5-fluorouracil towards cancer cells. We demonstrated facile modification of hydroxyapatite with curcuminoids and the potential of proposed nanostructural platform as therapeutic agent for effective cancer treatment presenting its interaction against biomimetic membranes and cancer cells.

2. Experimental

2.1 Materials and methods

The $Ca(NO_3)_2$ calcium nitrate (V), $(NH_4)H_2PO_4$ ammonium dihydrogenphosphate and 25% NH_3 ammonia solution with the analytical grade were purchased from POCH, Poland. Deionized water with resistivity 18.2 MΩ cm at 25 ˚C was obtained using the Milli-Q ultra-pure water filtering system (Merck, Darmstadt, Germany). The *Curcuma longa L.* rhizome powder was obtained from the curcumin powder supplied from Heuschen & Schrouff, Netherlands. Methanol used for curcuminoids extraction with >96% grade was supplied from Chempur, Poland and NaCl with analytical grade was purchased from Warchem, Poland. The 5-fluorouracil ≥99% grade was purchased from Sigma-Aldrich, Germany.

The following materials were used for cell experiments: McCoy's Medium, Eagle's minimal essential medium (EMEM), trypsin-EDTA, phosphate-buffered saline (PBS), fetal bovine serum, L-Glutamine, a penicillin/streptomycin solutions from Biological Industries (Biological Industries, Beth Haemek, Israel), and dimethyl sulfoxide (DMSO) (Sigma-Aldrich, St. Louis, MO, USA), CellTiter 96® Aqueous One Solution Reagent (MTS compound) from Promega (Promega, Madison, WI, USA).

A human-derived SKOV-3 cancer cell line was obtained from the American Type Culture Collection (ATCC, Rockville, MD, USA). It was cultured in McCoy's medium supplemented with 10% fetal bovine serum and 1% penicillin/streptomycin, where the cells were cultivated at 37 °C in a humidified atmosphere containing 5% CO_2. The HepG2 cell line was cultured similarly, while 1% L-glutamine was used in addition.

2.2 Synthesis of the hydroxyapatite

Hydroxyapatite (HAp) nanoparticles were prepared by co-precipitation within the procedure described as follows: 0.59 g of $Ca(NO_3)_2$ (calcium nitrate (V)) was placed into a beaker and dissolved in 5 mL of deionized water. The solution containing 0.33 g of $(NH_4)_2HPO_4$ diammonium hydrogen phosphate that was dissolved in the 5 mL of water, was put in the burette above the beaker that contained the solution of $Ca(NO_3)_2$. Also placed above the beaker is the another burrete that was filled with 25% ammonia solution.

To precipitate the HAp both solutions from the burettes were added dropwise to the beaker, where the ammonia was used as a precipitating agent. The pH during precipitation was adjusted to 11. After phosphates and ammonia addition, the suspension was stirred continuously for 4 h. Then, HAp suspension was washed with distilled water and centrifuged at 3500 rpm for 10 min. Washing of HAp was performed several times until reaching neutral pH.

2.3 Preparation of Curcuma longa L. rhizome extract

Curcuma longa L. extract was obtained within the extraction by use of the B-811 Büchi Soxhlet extractor (Switzerland). The 30 g of dry powder was placed in glass jar, where the methanol was added. The powder was extracted for at 80°C for 4 hours and then, the solvent was evaporated at 60°C overnight to obtain the *Curcuma longa L.* rhizome extract. The final product has t had the wax-like consistency containing mixture of various chemical compounds.

2.4 Modification of the hydroxyapatite

The 30 mg of curcumin extract was added into the 10 mL of HAp aqueous suspension and 30 mL of methanol was added to dissolve the extract. The suspension was continuously stirred with 500 rpm for 1 h, and then, placed into the Falcon tube, and centrifuged at about 2000 rpm for 5 minutes. Then, the solution above the HAp suspension was removed and replaced with water. Suspension was shaken for 2 minutes and sonicated for 5 min. After sonication the suspension was centrifuged to remove excess curcumine extract and the procedure was repeated three times.

The next step was loading of the 5-fluorouracil to curcuminoids loaded nanohydroxyapatite. 15 mg of drug was placed in the colloidal suspension and HAp@cur and stirred overnight with 300 rpm at room temperature. Then, the suspension was centrifuged at about 2000 rpm for 5 min, washed with Milli-Q water, and centrifuged again. Finally, the suspension was suspended in 30 mL of water, where the suspension was shaken on a vortex for 3 minutes.

2.5 Cytotoxicity studies

Prior to the cells treatment with the proposed nanocomposite and particular ingredients of the composite, the cells (2.5×10^3 SKOV-3, 10×10^3 HepG2) were seeded in 96-well plates and incubated

under 5% CO_2 atmosphere at 37 °C. Then, the medium was removed, compounds were added and incubated for 24 h and 48 h. After a suitable time, the medium with compounds was removed, the wells with cells were washed with PBS and fresh medium and MTS reagent were added. After two hours of incubation, the absorbance was measured at 490 nm and the cell viability was calculated.

2.6 Characterization

The extraction of turmeric was performed using B-811 Büchi Soxlet extractor (Switzerland). Curcuminoid analysis was performed using a Shimadzu UFLCXR liquid chromatograph with a detector with SPD-M30A photodiode array. UV-Vis spectra were acquired from 200-800 nm. A Phenomenex Luna 3u C18 (2) 100A (150 x 3.0 mm) column was used for HPLC analysis. Column temperature was set to 48°C. The gradient elution profile was as follows: (A) water (0.25% HOAc) and (B) acetonitrile, 0-17 min, 40-60% B, 17-28 min, 60-100% B; 28-35 min, 100% B; 35–40 min, 100–40% B at a flow rate of 0.8 $mL \cdot min^{-1}$.

The turmeric extract was also tested on an Agilent 7890B GC System gas chromatograph with an Agilent 5977B GC/MSD mass spectrometry detector. An HP-5MS column (0.25 mm x 30 m x 0.25 μm) was used for the tests. The analyzes were performed under the following chromatographic conditions: injector temperature 250°C, detector temperature 280°C, oven temperature program from 50°C/4 min - increase of 15°C min to 300°C (maintained for 10 min). Helium was used as a carrier gas, gas flow was set at 1 ml/min. The volume of the dosed sample was 1 μL. The substances were identified by comparing the obtained MS spectra with the spectra of the NIST17.L Mass Spectrum Library.

The characterization of chemical moieties in the extract was carried out by Fourier-transform infrared spectroscopy (FT-IR) using the ATR technique (Alpha ~~apparatus) supplied~~apparatus) supplied from Bruker. The measurements were ~~perfomed~~performed in the range of 4000–400 cm^{-1}, where the 32 scans at a resolution of 4 cm^{-1} were performed.

The morphology studies were performed by the Scanning Electron Microscopy (SEM) — Merlin, ZEISS, Stuttgart, Germany and Transmission Electron Microscopy (TEM) — Zeiss Libra 120 Plus, Stuttgart, Germany, operating at 120 kV. Hydrodynamic diameter and the zeta potential of the particles were measured with a Malvern Zetasizer instrument (Nano ZS, UK) fitted with He-Ne laser ($\lambda = 632.8$ nm) as the light source at the scattering angle of 173°, where the ionic strength was adjusted with NaCl to 0.01 M in case of the surface potential determination.

The stability of the obtained composite was carried out using the multiple light scattering method by Turbiscan Lab apparatus (Formulaction SA, France), where the colloidal suspension of HAp in water was placed in glass cylindrical measurement test tubes with a working height of 54 mm. Then, the samples were placed in a Turbiscan Lab apparatus (Formulaction SA, France) and subjected to scanning with light at a wavelength of about 880 nm. The scans were carried out every 5 minutes for half an hour at room temperature (23 °C). Based on the obtained results, the Turbiscan Stability Index (TSI) was determined.

The X-ray diffraction analyses (XRD) were performed using the DSH method on a Malvern

Panalytical X'Pert PRO MPD powder diffractometer. The XRD patterns were recorded in the (2θ) range from 18° to 85°, with a scan rate of 1 °per minute with total record time of 67 minutes. Analysis were done with using Co Kα at 40 kV and 40 mA. Phase identification was obtained with the use of X'Pert Plus HighScore software with access to the COD (Crystallography Open Database) database. The crystallite sizes were calculated using a Scherrer formula.

The Langmuir trough and barriers were cleaned with chloroform and methanol to remove potential impurities before each measurement. Wilhelmy's platinum plate was flamed to remove all contaminants from the surface. The trough was filled with the subphase solution (milli-Q water or solution of drug/carriers), and then, 30-40 µL of a chloroform solution of the selected lipid at a concentration of 2 $mg \cdot mL^{-1}$ was dropped. After about 15 minutes, when the solvent had evaporated, the layer was compressed. The experiments were carried out with a 5 $cm^2 \cdot min^{-1}$ barrier movement speed until the surface pressure reached the value 30 $mN \cdot m^{-1}$.

2.7 Statistical analysis

To analyse the experimental data, GraphPad Prism version 8.0 software (GraphPad Software Inc., San Diego, CA, USA) was applied. Values between groups were compared using one-way ANOVA. The results are presented as mean ± standard error of the mean (SEM) and were considered as statistically significant when $p \leq 0.05$, $p \leq 0.01$, $p \leq 0.001$, and $p \leq 0.0001$.

3. Results and discussion

3.1 Curcumin extract characterization

As-prepared extract was investigated with the high-pressure liquid chromatography to determine the compounds that are present in the extract. The results indicated that the extract contain biologically active molecules. The type A turmeric extract was used for the research, which characterizes that curcumin was the most common compound, and the sum of the content of demethoxycurcumin and bisdemethoxycurcumin was lower than curcumin. From the HPLC analysis, it can be concluded that the three major curcuminoids are sorbed on the hydroxyapatite (Fig. 1a). On the basis of comparison with reference materials, bisdemetoxycurcumin (1) with a retention time of t_R = 6.154 min, demethoxycurcumin (2) with a t_R = 6.764 min, and curcumin (3) with a t_R = 7.404 min were identified.

Based on the GC-MS analysis (Fig. 1b), it was found that also the following compounds are sorbed ar-curcumene (4), (-)-zingiberene (5), b-zesquiphelandrene (6), b-turmerone (7), (6R,7R)-bisabolene (8), (E)-atlantone (9). All of these compounds reveal biological activity [], [], [], [].

Table 1 shows the selected m/z signals of the identified compounds marked on chromatograms as 1-9.

Commented [p7]: https://www.frontiersin.org/articles/10.3389/fphar.2022.820806/full

Commented [p8]: https://www.mdpi.com/2223-7747/11/15/1932

Commented [p9]: https://www.mdpi.com/2073-4395/12/5/1168

Commented [p10]: https://link.springer.com/article/10.1007/s12325-022-02081-w

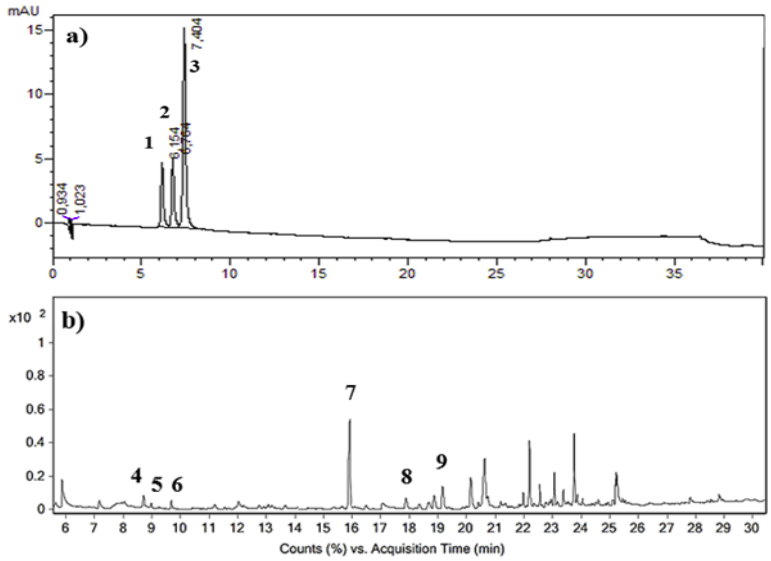

Figure 1. Chromatograms of turmeric extract sorbed on hydroxyapatite: a) HPLC analysis, b) GC-MS analysis

Table 1. List of compounds with selected m/z signals

Signal	t_R	Name of compound	Selected m/z signals (% of base peak)
4	8.712	ar-Curcumene	105 (56), 119 (100), 132 (74), 202 (24)
5	8.973	(-)-zingiberene	69 (40), 93 (100), 119 (94), 204 (10)
6	9.685	b-sesquiphelandrene	69 (100), 93 (50), 133 (20), 161(20), 204 (10)
7	15.949	b-turmerone	55 (20), 83(40), 105 (19), 120 (100), 218 (5)
8	17.879	(6R,7R)-bisabolene	95 (45), 110 (58), 137 (100), 204 (10)
9	19.16	(E)-atlantone	83 (100), 123 (35), 135 (42), 203 (20), 218 (10)

Comparing the composition of compounds that was adsorbed on hydroxyapatite with the crude turmeric extract (Fig. 2) used for the research, it can be concluded that only ar-turmerone (10) and a-turmerone (11) were not sorbed on the mineral. Both the composition of sorbed substances on hydroxyapatite and turmeric extract is similar to the compounds identified by Li (Li et al., 2010) and Xu (Xu et al., 2020).

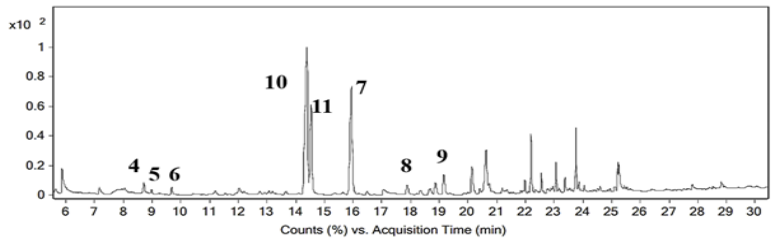

Figure. 2. GC-MS chromatogram of crude turmeric extract: ar-Curcumene (4), (-)-zingiberene (5), b-sesquiphelandrene (6), ar-turmerone (10), a-turmerone (11), b-turmerone (7), (6R,7R)-cisabolene (8), (E)-atlantone (9).

3.2 Morphology studies

The morphology of prepared composites was studied with Scanning Electron Microscope (SEM) and Transmission Electron Microscope (TEM). SEM images are presented in Fig. 3 in the left column, while TEM images are presented in the right column. As can be seen in Fig. 3a bare HAp ~~shows agglomeration~~shows agglomeration of nanoparticles of irregular shape and spiky structures, while TEM images (Fig. 3b) ~~reveal needle~~reveal needle-like agglomerates that look like round shaped objects. Due to the drying of HAp within the stabilizers the particles tend to agglomerate, so the morphology is difficult to be determined for the overlapping of the particular grains. Following Fig. 3c-d reveal the HAp modified with curcuminoids. SEM image shows similar morphology full of bulky clusters. However, TEM analysis confirms the needle -like structure of the HAp similarly to the structures described in literature (Mujahid et al., 2015; Núñez et al., 2019) Modified HAp less aggregate than bare HAp. After the loading of the 5-fluorouracil into the HAp@cur structures the composite looks similar like after the initial modification with curcuminoids. As can be seen in Fig. 3 e-f the needle like structures are also revealed that occur within the whole sample, where the average diameter of a rod is about 12 nm and 70 nm in length.

a)	b)

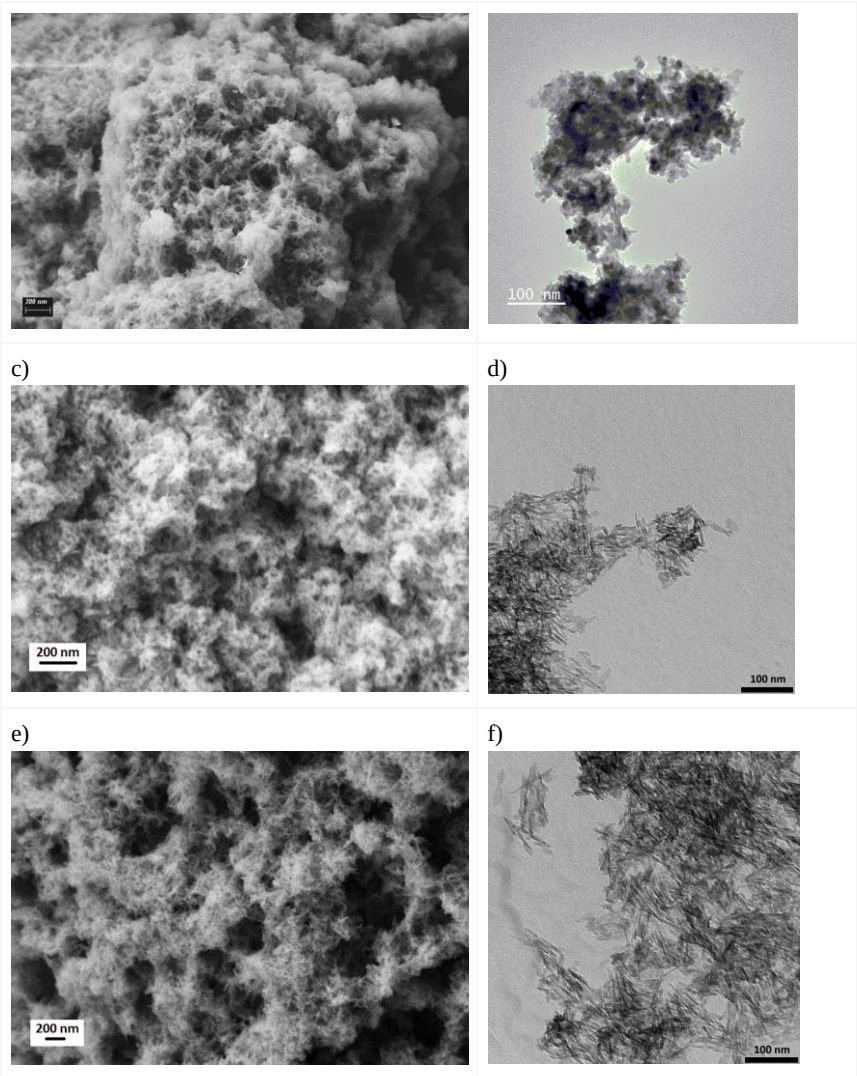

Fig. 3. a) SEM and b) TEM images for HAp, c) SEM, d) TEM images for HAp@cur composite, and e) SEM, f) TEM images of HAp@cur@5-flu.

3.3 Hydrodynamic size, crystallinity of Hap, and adsorption capacity

Complementary to the TEM analysis, DLS studies have shown the hydrodynamic size of the curcuminoids and drug loaded composite of about 70 nm Fig 4a. Then, the surface charge was

determined, where the bare HAp has -9.4 mV surface charge. The zeta potential for the HAp loaded with curcuminoids was about 7.3 mV indicating that the particles were positively charged. The change of the surface potential corresponds to the presence of the curcuminoids-based and drug-based functional groups. Despite the low value of the zeta potential, due to the repulsion forces the colloidal suspension remains stable.

The structure of prepared HAp was investigated with XRD technique based on recorded patterns. Figure. 4b confirms the presence of reflections peaks at 20.07, 24.91, 27.23, 32.03, 33.68, 40.20, 43.66, 45.16, 48,92, 52.55, 57.63, 60.04, and 66.89° corresponding to its main diffraction planes: (200), (002), (207), (211), (300), (310), (311), (203), (222), (104), (322), (420), and (304), respectively (), (), (). that were also identified based on the 96-901-1092 card from the Crystallography Open Database (COD). The size of crystallites is ranging around a few dozens of nanometers, which is also confirmand by electron microscopy studies

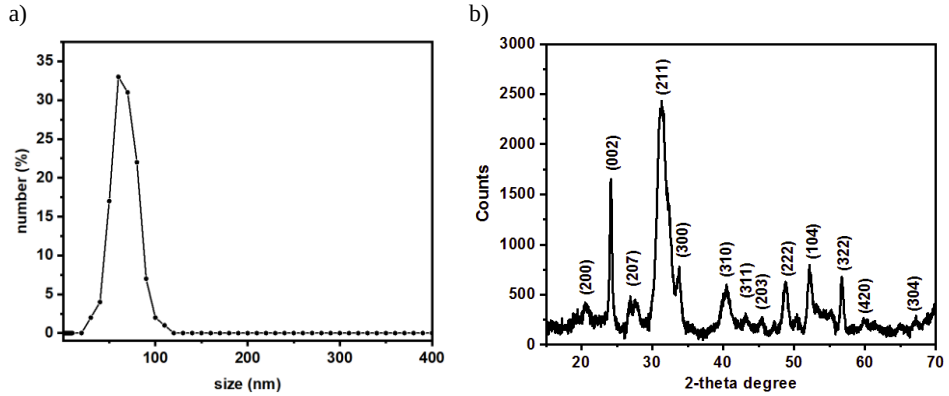

Fig. 4. a) distribution of size (hydrodynamic diameter) hydrodynamic size, and b) XRD pattern for HAp, recalculated to standard references for Cu cathode.

The specific surface area of hydroxyapatite structures was determined by the Brunauer-Emmett-Teller (BET) method, using nitrogen adsorption at 77 K (Figure 4). Figure 5 shows the characteristic N_2 adsorption/desorption isotherm revealing a typical type IV isotherm curve with a hysteresis loop. It points out the presence of mesopores (Nguyen et al., 2020; Shaban et al., 2018) where the average size of pores is 14.54 nm. The material shows the specific surface about 105.0222 ± 0.7608 m^2g^{-1} confirming the high adsorption capacity making it possible to load cucrcumine extract and the drug for further in vitro studies. This BET specific surface area obtained is this study is higher than 32 m^2g^{-1} that had been earlier reported for HAp in another study (Ayodele et al., 2021)

Commented [p11]: https://link.springer.com/article/10.1007/s11696-021-01841-2

Commented [p12]: https://link.springer.com/article/10.1007/s10832-021-00274-3

Commented [p13]: https://www.researchgate.net/publication/362196252_Green_Synthesis_of_Hydroxyapatite_Nanoparticles_from_Wrightia_tinctoria_and_Its_Antibacterial_Activity

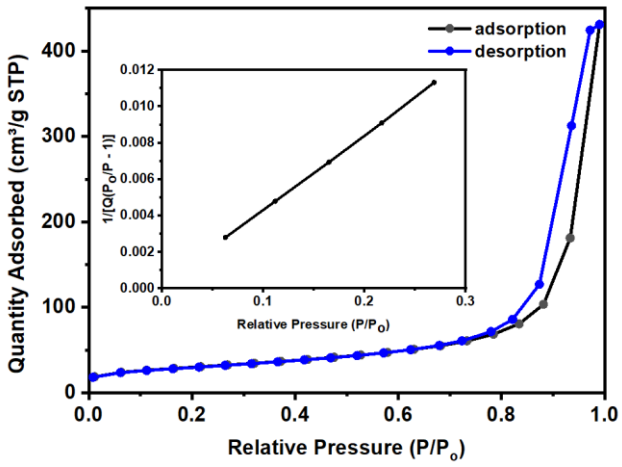

Fig. 5 The N_2 adsorption isotherm for the HAp

3.4 Chemical composition and content of organic compounds

Curcumin extract was characterized with FT-IR technique. As can be seen in Fig. 6a the -CH_2 asymmetric stretching and C-H aromatic stretching vibration are shown by the bands at about 2924 cm^{-1} and 3015 cm^{-1}, while the broad band at about 3347 cm^{-1} corresponds to the -O-H stretching vibration. The following peaks at about 1376 cm^{-1}, 1442 cm^{-1}, 1511 cm^{-1} can be ascribed to the CH_3 bending, CH_2 bending, and benzene ring bending vibrations. Following peak 1678 cm^{-1} comes from the C=O stretching, and 1581 cm^{-1} is characteristic to the C=C aromatic stretching. The peak ~~at about~~at about 1029 cm^{-1} is characteristic of C-O-C, while peaks at 1124 and 1271 cm^{-1} can be ascribed to the C-O stretching and enol C-O peak, respectively. The 815 cm^{-1} and 815 cm^{-1} peaks correspond to the -CH aromatic bending and benzoate trans-CH vibration are apparently seen. Recorded data are in good agreement with the literature (Chen et al., 2015; Ismail et al., 2014) Next, the analyses were performed for the HAp, HAp@cur, and HAp@cur@5-flu.

The FTIR spectra of HAp, HAp@cur, and HAp@cur@5-flu can be seen in Fig. 6b the peaks in the range 500-600 cm^{-1} can be ascribed to PO_4^{2-} groups. The following bands at 1000-1200 cm^{-1} are also characteristic to these groups cm^{-1} (Gheisari et al., 2015; Slosarczyka et al., 2005). The 1620 cm^{-1} band comes from the bending vibration of water, while the intralayer H-bonded and also O-H stretching can be ascribed to the broadband centered at 3400 cm^{-1}. The bands at 2920 cm^{-1} and 2850 cm^{-1} can be ascribed to the presence of C-H vibration from the organic compounds coating HAp (Zuo et al., 2011). Due to the presence of 5-flu the following bands can be ascribed: 1725 cm^{-1} for the cyclic imide, CONHCO), 1672 cm^{-1} for imide, amide I band (C=O), and 1247 cm^{-1} for amide III band (C-O) (Gupta et al., 2014; Jin et al., 2014, 2010)

a) b)

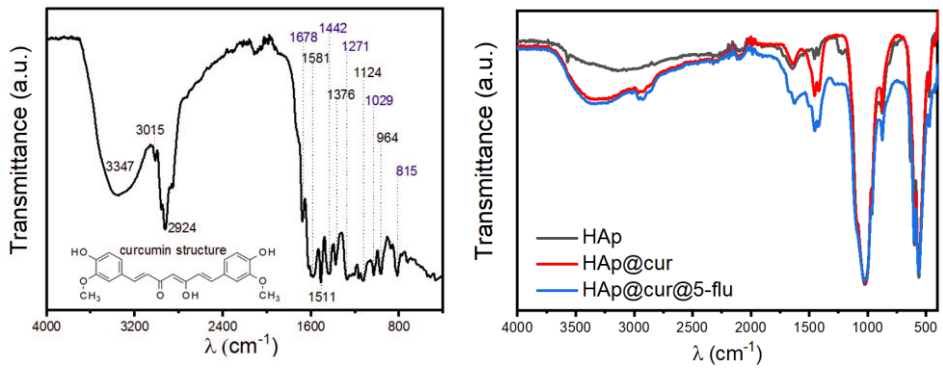

Fig. 6 FT-IR spectrum of a) curcuminoids extracted from curcumin and HAp, Hap@cur, and Hap@cur@5-flu.

3.5 Turbiscan analysis

The stability of the nanocomposite-based suspension was investigated with the multiple light scattering method, namely turbiscan method. It makes it possible to determine the flocculation, aggregation, or sedimentation of tested material etc. (Dai et al., 2015; Lili et al., 2017; Zhong et al., 2016). The sample plots presented in Fig. 7 show percentages of transmitted light (ΔLT) and backscattered light (ΔBS) over the 1.5 mg mL^{-1} vs. hight of the sample for HAp suspension in distilled water. Based on the turbiscan analysis it is seen that the prepared suspension was stable (T=0%) at initial observations., while the transparency increase and raise of the backscattered light intensity over time was observed at the top of the sample indicating partial sedimentation of the nanocomposite-based suspension (Lee et al., 2016; Qi et al., 2017), see Fig 8a. This is confirmed by the densification of the lower suspension layer, over time which is manifested by an increase in the BS intensity, in the lower part of the sample, see Fig. 7b. (). Suspensions of both HAp@cur and HAp@cur@5-flu nanocomposites underwent the same destabilization mechanism.

a) b)

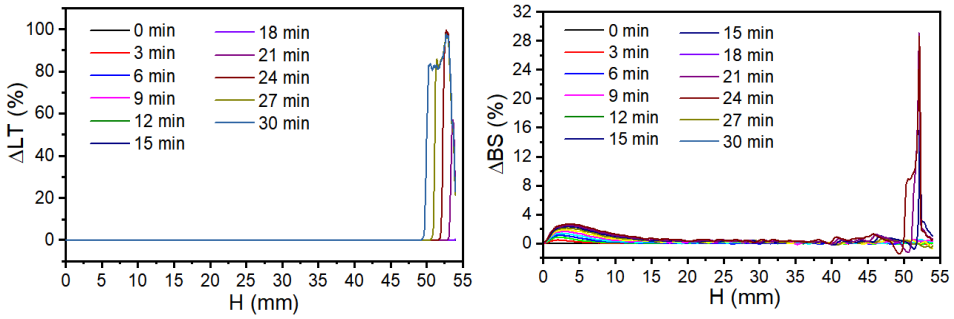

Fig. 7 a) percentages of transmitted light over the height of the sample, b) percentage of backscattered light over the height of the sample.

On the basis of the obtained results of the stability of nanocomposite suspensions, the destabilization kinetics of the prepared systems was determined (see Fig. 8). For this purpose, the Turbiscan Stability Index (TSI) was determined with the help of software supplied by the manufacturer. The TSI is the most efficient method of quantitative comparison of several systems between each other. The TSI value is higher the more the system is unstable (Dai et al., 2015; Ren et al., 2018). Due to the destabilization mechanism (sedimentation), the TSI was determined in the upper part of the sample (H = 36-54 mm), where the changes in the stability of the systems were most noticeable, see Fig. 8a. On the basis of the results, it was found that HAp@cur, HAp@cur@5-flu are stable suspensions in water. The use of the *Curcuma longa* L. rhizome extract improved the HAp stability as well as the 5-fluorouracil loading what is required to be used in the following *in vitro* studies.

The thermogravimetric analysis (TGA) was performed to estimate the content of organic compounds in the HAp matrix. The TGA measurements of the gradual mass loss while heating were performed in the ambient atmosphere in the temperature range from the 50 ˚C temperature to 600 ˚C, with the heating rate of 10 ˚C/min, see Fig. 8b. Gradual mass loss is observed in the thermogram of HAp from 50 ˚C to 200 ˚C which is due to loss of bound water. The increase in temperature after 200 ˚C did not insignificantly lead to loss of mass. This implies that HAp is relatively thermally stable at the temperature above 200 ˚C.

In the case of HAp@cur and HAp@cur@5-flu the presence of organic molecules (Curcumin extract and 5-fluorouracil), led significant mass loss when the temperature was above 200 ˚C. The mass loss of HAp@cur and HAp@cur@5 from above 200 ˚C was due to the decomposition of both Curcumin extract and 5-fluorouracil that were loaded in the HAp matrix.

As can be seen in thermogram the content of Curcumin extract is about 14%, while after the 5-fluorouracil loading, drops of about 2% due to the decomposition of drug was observed

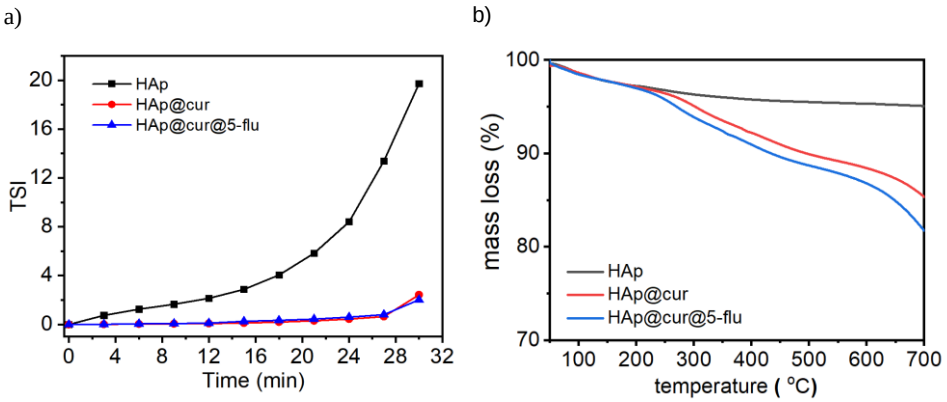

Fig. 8 a) Turbiscan Stability Index change in time and thermograms and B) TGA curves for HAp, HAp loaded with curcuminoids, and HAp loaded with curcuminoids and 5-fluorouracil.

3.6 Influence on biological membranes

Following studies were performed the influence of various substances on the biological membranes within the Langmuir trough. The biomimetic membranes prepared during the experimental work are an ~~analogues of the biological membranes~~analogue of the biological membranes ([i], [ii]). The Langmuir technique enables the formation of such ~~analogs that~~analogs that ~~are more~~are more easily controllable in composition than the natural membranes and testing their interaction with the drug carriers ([iii]).

The monomolecular layers were created on the Langmuir trough with the use of three types of lipids: DOPC (1,2-dioleoyl-sn-glycero-3-phosphocholine), DOPE (1,2-dioleoyl-sn-glycero-3-phosphoethanolamine) and cardiolipin. The choice of lipids was carefully considered due to their differences in the acid-base properties and the structure of fatty acid chains. The subphases in these studies were as follows: water, 5-fluorouracil solution, and hydroxyapatite suspensions including bare HAp, HAp loaded with curcuminoids, and both, curcuminoids and anticancer drug. Comparative isotherms have not been recorded for pure curcumin extract due to partially hydrophobic properties. At the beginning the influence of HAp on the resulting biomimetic layers was investigated. Plots of ~~the surface~~the surface pressure (π) as a function of surface area (A) for a single lipid molecule, called π-A isotherms are shown in Fig. 9.

The Fig 9a shows the recorded isotherms for DOPC lipids. It turns out that the addition of only a small amount of pure hydroxyapatite causes the curve shift by about 22%. The use of a higher concentration of the carrier does not affect the lipid organization so significantly, which may indicate that the carrier accumulates in the lipid layer only in a specific concentration range. The explanation of this phenomenon may be related also to the possible precipitation of hydroxyapatite from the solution at high concentration values. The modification of the nanocarrier with curcumin causes a

significantly lower increase in the surface area/particle compared to the subphase with pure carriers. The addition of a lower concentration of modified hydroxyapatite increases the surface area by approx. 25%. These values are similar for both concentration of the carrier with curcumin. It is noticeable that the addition of curcumin reduces the interaction between the lipid and the components of the subphase and affects the way of accumulation of the carrier in the lipid structure. These changes in the course of isotherms may also be related to the higher stability of the nanosystem after modification with curcuminoids.

It has been observed that the change in surface pressure is caused by a change in the physical state of the monolayer and, consequently, by a change in the rheological properties of the monolayer ([iv]). Generally, the concept of compressibility (C_s) is defined, which is described by the equation (1):

$$C_s = -\frac{1}{A}\left(\frac{dA}{d\pi}\right)_{T,p} \qquad (1)$$

Where A is Area (m) and π is surface pressure ($mN \cdot m^{-1}$).

The much more commonly used term is the compressibility factor, which is the reciprocal of the compressibility ([v]). By analyzing the experimental data, the ranges of the values of the compressibility coefficients corresponding to the individual physical properties of the monolayer were determined. Based on the π-A isotherm, it is possible to estimate the value of the compressibility coefficient (C_s^{-1}), while the plotting the dependence of this coefficient on the surface pressure (π) allows to determine the maximum value of the compressibility coefficient showing the degree of ordering of molecules in the monolayer at the water/air interface. By using values of the compressibility ~~coefficient~~coefficient, it is possible to determine the physical state of the monolayer in accordance with the Davies and Rideal criteria ([vi]).

The values of the compressibility coefficients of the DOPC layer as a function of the surface pressure for different subphase composition are presented in the Fig. 9b diagram. It can be concluded that for all measurements, the values of the compressibility coefficients are constantly increasing, which means that phases change during lipid compression are not noticeable in the isotherms. The compressibility coefficients assume similar values of approx. 110 $mN \cdot m^{-1}$ (at p = 30 $mN \cdot m^{-1}$), which suggests that the liquid condensed state was achieved.

In the next stage, the influence of ~~modified with~~modified with 5-~~fluorouracil (~~fluorouracil (FU) and curcumin hydroxyapatite on the formed biomimetic layers was studied. As a result of the measurements, the isotherms presented in the figure Fig. 9a (magenta curve) were obtained. The addition of fluorouracil to the subphase causes an accumulation of the drug in the area of hydrophilic lipid heads (about 10%), which is expressed by increasing the surface area per DOPC molecule. Changing the concentration of the drug has no influence on this effect, the isotherms for both ~~concentrations (~~concentrations (C_1 10^{-6} M and C_2 10^{-7} M) converge (data not showed). It turns out that the modification of ~~hydroxyapatite by~~hydroxyapatite by drug contributes ~~to different~~to ~~adsorption~~different adsorption in the layer of 5-fluorouracil, there is a slight isotherm shift (about 7%) in relation to the subphase with pure anticancer drug. The drug is incorporated into the interior

of the carrier by the adsorption process in the pores of hydroxyapatite. The functional groups of the therapeutic are not blocked by a chemical bond however, some of them may be hidden within the carrier structure and thus it may have an influence on the interaction with the membrane.
The addition of a drug or drug-modified carrier to the subphase causes significant changes in the value of the compressibility coefficient. The presence of the drug reduces these values to about 60 $mN \cdot m^{-1}$, which is associated with a change in the organization of lipids and the formation of an expanded liquid phase. This is also confirmed by the different slope of Langmuir isotherms (for FU and FU-HAp) suggesting greater fluidity of the membrane in the presence of the therapeutic.

The second lipid used in the research was DOPE, a compound characterized by a functional group with basic properties. The Π-A curves obtained as a result of compression of the DOPE lipid monolayer are presented in the Fig. 9c figure. The influence of pure hydroxyapatite on the structure of the DOPE membrane is related to the adsorption of nanostructures in the area of the hydrophilic part of the film. However, the isotherms recorded for different concentrations of the pure carrier and its forms with curcumin show slight shifts in the graph. It can be concluded that for this effect, the concentration of the carrier and the contact time with the membrane are irrelevant. 5-Fluorouracil strongly interacts with the ~~membran~~membrane~~e~~. On the isotherm, it is visible as a shift of the curve to the left, which may be related to a different angle of the lipid position in relation to the water surface.

The presence of a drug concentration 10^{-6} M in the ~~subphase decreases~~subphase decreases the surface area by about 12%. Too strong accumulation in the membrane is not a favorable phenomenon because it may limit the penetration of the therapeutic into the cell. The use of a fluorouracil carrier may contribute to weaker adsorption of the compound that will be locked inside the nanostructure. Based on the recorded isotherms, it can be seen that the incorporation of the drug inside the hydroxyapatite structure results in a lower accumulation of such conjugate in the membrane DOPE (characterized by the presence of amino groups).

Binding of the drug to the carrier reduces its affinity for the polar part of the lipid layer, as the surface area increases in relation to the free drug. In the case of a higher concentration of the carrier with the drug, the surface area is reduced by approx. 10%, and for a lower concentration - by approx. 9% (data not showed), which means that along with the reduction of the amount of the drug-modified carrier in the subphase, its interactions with biomimetic membranes decrease.

The values of the compressibility coefficient for almost each of the isotherms are about 110-115 $mN \cdot m^{-1}$ and correspond to the ~~boundary liquid~~boundary liquid condensed phase (Fig. 9d). These results point out to similar interactions between the DOPE lipid and the hydroxyapatite conjugate. Some reorganization in the monolayer is seen in the presence of free drug in the subphase. The compressibility coefficient is about 90 $mN \cdot m^{-1}$ which indicates a change in the phase state. It is probably associated with strong interactions between the anticancer drug and the lipid during the compression of the layer.

The last of the examined lipids was cardiolipin - a ~~lipid with~~lipid with acidic properties of polar head (Fig. 9e). The content of a small concentration of hydroxyapatite in the subphase causes

an increase in the surface area per molecule by about 15%, but there is no correlation with the concentration of hydroxyapatite. The adsorption of curcumin in hydroxyapatite contributes to a significant reduction of the surface area on the isotherm (by approx. 13% in the case of a lower concentration of the modified carrier and by approx. 17% in the case of a higher concentration of the modified carrier). Probably, curcumin, by changing the surface properties of the carrier, contributes to the reduction of penetration of nanostructures into the membrane, the same as in most of the tested layers.

Therapeutic in the range of high concentrations (10^{-6} M) accumulates in the cardiolipin layer not so strong as anthracycline ([vii]). The encapsulation of the fluorouracil in hydroxyapatite does not reduce the degree of adsorption of the compound in the region of the hydrophilic polar groups of the lipid compared to the free drug. Modification of the carrier with a therapeutic agent causes visible changes in the slope of the isotherm, which suggests a change in the fluidity of the layer.

Based on the values of the compressibility coefficients, it can be seen that the membrane made of cardiolipin molecules is in the expanded liquid phase (about 70 $mN \cdot m^{-1}$). The membrane organization is changed in the presence of the hydroxyapatite in the subphase (especially high concentration), because under these conditions the value of the compressibility coefficient increases to about 86 $mN \cdot m^{-1}$. It is related to the change in the organization of lipids and the increase in the degree of ordering of the layer towards the condensed liquid phase. Subphase modification ~~by drug~~by drug or HAp with drug contributes to increase in the C_s^{-1} value to 41 and 61 $mN \cdot m^{-1}$, respectively.

a)

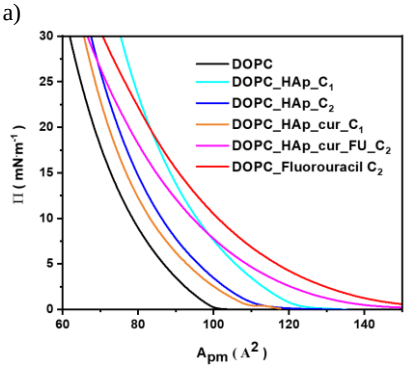

b)

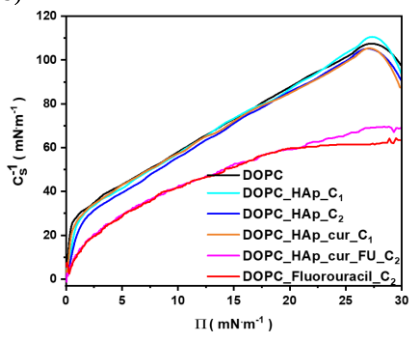

c)

d)

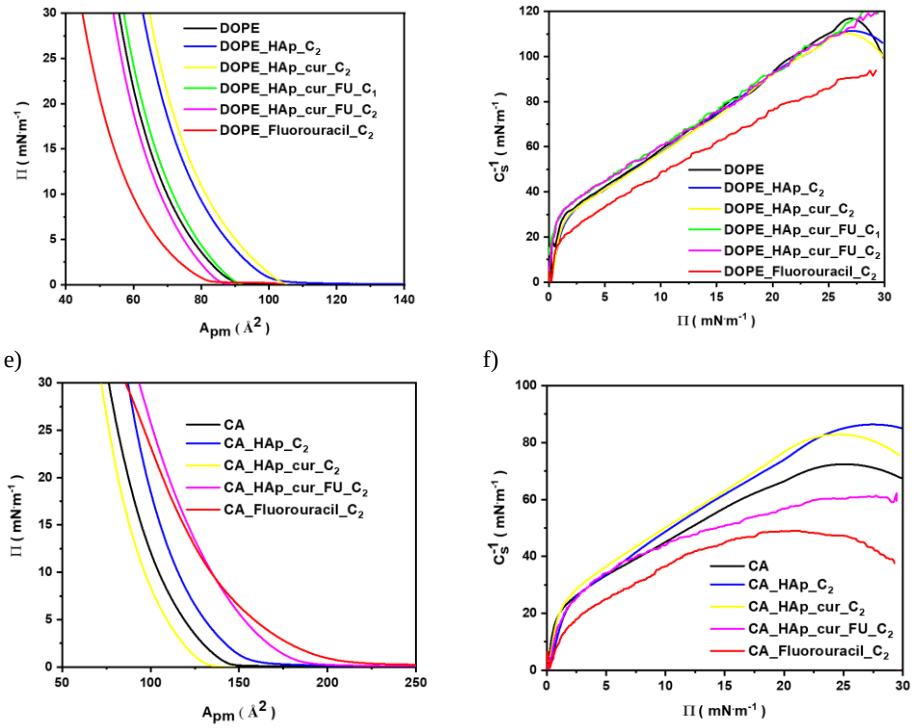

Fig. 9. Langmuir isotherm (a, c, e) ~~and compressibility~~and compressibility coefficients (b, d, f) for lipids: DOPC, DOPE and cardiolipin (CA); measurement conditions marked on the graphs

The surface pressure – area per molecule measurements allowed us to monitor the effect of hydroxyapatite and their conjugates on the structure of monolayers formed by the selected phospholipids. The results of those studies showed the degree of incorporation of the drugs or compounds and their conjugates into the layers and changes in the properties of the ~~monolayers upon~~monolayers upon compression in the presence of the nanosystem.

The results have shown the ability of modified ~~hydroxyapatite to~~hydroxyapatite to interact with and/or to insert among phospholipid molecules in membrane especially in the presence of choline. In this case, even a small addition of a pure carrier significantly influences the isotherm shift. The presence of curcumin changes the surface properties of the conjugate, which contributes to the low affinity of the nanocarrier to most of the tested membranes. The obtained results suggest that fluorouracil has a strong affinity for the most used lipid However, drug adsorption with hydroxyapatite significantly reduces this type of drug-lipid interaction. For most of the tested lipids, the addition of the conjugate changes the fluidity of the membrane. A decrease in the compressibility

coefficients in the presence of a drug or ~~drug with~~drug with hydroxyapatite contributes the modification in membrane fluidity ~~and can~~and ~~alter~~can alter functional properties ~~of membrane~~of membrane. Moreover, pathological processes in living cell can also be related to fluidity modifications.

The effect of drugs nanocarriers on the structure of cell membranes is an important part of the overall effectiveness of conjugates. These effects can be studied systematically using model membrane systems. Langmuir monolayer provide the advantage of a system with reduced complexity and control over the individual constituents. While model membranes will never be able to entirely replace in vitro studies, they can provide a useful first screening platform for the investigation of nanosystem–membrane interactions. Therefore, the following studies included *in vitro* tests.

3.7 In Vitro Cytotoxicity Results

Following, the cytotoxicity studies with the use of MTS colorimetric assay were performed, where the composite and bare components were tested. To determine cytotoxic effect on cells, they were incubated with various concentrations (50, 100, 200 µM) of HAp, curcuminoids, 5-flu, HAp@cur, and @HAp@cur@5-flu for 24 h and 48 h. The viability of the control group of SKOV-3 and HepG2 was set to 100%. As can be seen in Fig. 10 the hydroxyapatite was not toxic up to 100 µM, similarly to the literature [], whereas higher concentration (200 µM) decreased the viability to ~85%. It can be caused by the agglomeration of the HAp onto the cells []. Several literature studies indicate the correlation between the size and shape of HAp and its cytotoxicity (), (), (). For example Huang et al. present that the cytotoxicity of HAp is affected by various physical parameters, electrical conductivity, surface potential, and specific surface area (). The addition of free curcumin to cells, did not cause any cytotoxicity even at very high concentration 200 µM. Interestingly, bound curcumin to HAp decreased slightly the viability, but only of SKOV-3 cells at high concentrations. It can also be noticed that 5-fluorouracil and HAp@cur@5-flu cytotoxicity increased in time and concentration dependent manner. In the case of ovarian cancer cells, which were treated with 5-fluorouracil attached to HAp@cur, the viability was higher than for cells treated with only free chemotherapeutic. It is in agreement with our previous studies where other cytostatic drug – doxorubicin bound to SPION@CA nanoparticles was used (). On the contrary, these results were not similar for HepG2 cells, where after 24 h and 48 h of incubation, the cytotoxicity of 5-flu was lower than HAp@cur@5-flu. The results clearly indicate that nanocpmposite loaded with curcumin extract and anticancer drug exhibits cytotoxicity for SCOV-3 and HepG2 cancer cells at presented concentration and incubation time than this drug bound to HAp@cur@.

Commented [p14]: In Vitro Biocompatibility Assessment of Nano-Hydroxyapatite doi: 10.3390/nano11051152

Commented [p15]: https://www.sciencedirect.com/science/article/abs/pii/S014296120900235X?via%3Dihub

Commented [p16]: https://www.sciencedirect.com/science/article/pii/S174270610800216X?casa_token=Uw84a4dUwgAAAAA:Qr3nWd8ZY7DY_ZGKZrZ4KZsTI78jn-WVAzlcyO_Sr3tqPF3iyk6A1dlQXFPupaY2uX2zUhu9QGg

Commented [p17]: https://www.ncbi.nlm.nih.gov/pmc/articles/PMC3075893/

Commented [p18]: https://www.sciencedirect.com/science/article/pii/S092849311930178X?casa_token=OJSg1TH6rUMAAAAA:vmgXYd1wQ8mL05sPVgBhyqJqKAezuCHDBofAaUSn4mV40INgSjefNBky6dMAro59GOV8DgFKlK0

Commented [p19]: https://www.nature.com/articles/s41598-019-55428-9

Commented [p20]: Nieciecka, D.; Celej, J.; Żuk, M.; Majkowska-Pilip, A.; Żelechowska-Matysiak, K.; Lis, A.; Osial, M. Hybrid System for Local Drug Delivery and Magnetic Hyperthermia Based on SPIONs Loaded with Doxorubicin and Epirubicin. Pharm. 2021, 13.

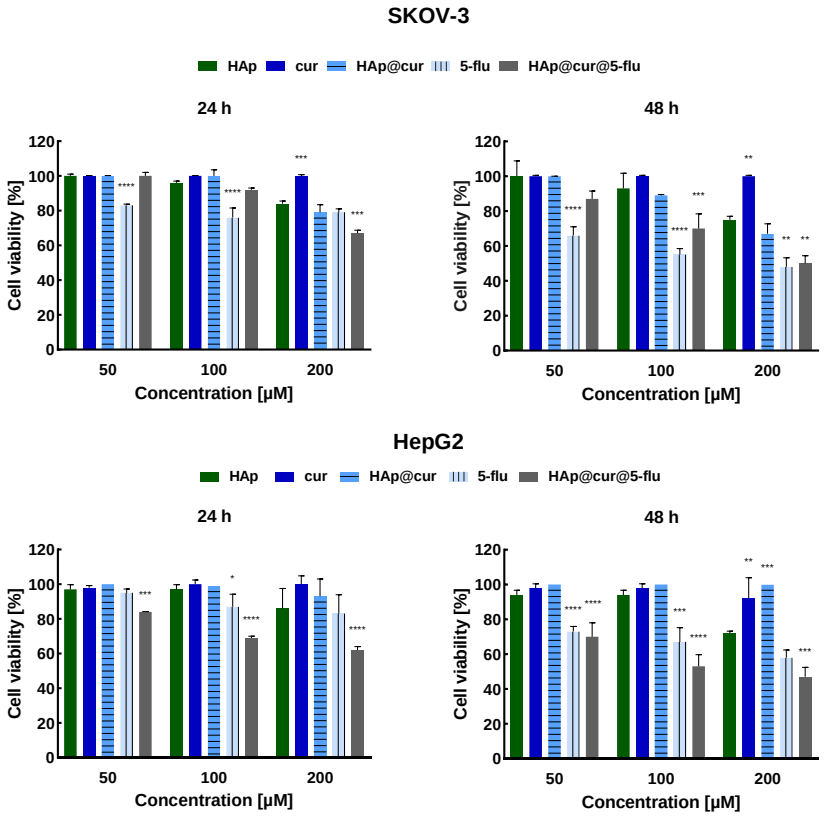

Figure 10. Cytotoxicity studies performed on SKOV-3 and HepG2 cells treated with various concentrations (50, 100, 200 µM) of HAp, cur, HAp@cur, 5-flu, HAp@cur@5-flu after 24 h and 48 h of incubation. Data points and SD are from at least three measurements. Statistical significance was considered if $p \leq 0.05$ (*), $p \leq 0.01$ (**), $p \leq 0.001$ (***), $p \leq 0.0001$ (****).

Conclusions

In this work, the nanostructured hydroxyapatite was synthesized with co-precipitating method as a porous platform for drug delivery. HAp was obtained in rod-like shape and nanometric size offering large surface-to-volume ratio and stabilized with curcuminoids extracted from *Curcuma longa L.* rhizome. The extract was used for its enriched composition in contrast to the commercially available curcumin, containing even nine biologically active compounds. The chemical composition of the extract was studied with HPLC and GC confirming the revealing presence of even nine biologically active compounds. The extract was proposed to improve the anticancer effect of the composite, while

it also worked well as a stabilizing agent of nanocomposite. Proposed nanocomposite was also loaded with 5-fluorouracil anticancer drug and the nanocomposite was tested within the Langmuir trough to determine the interaction of the nanocomposite with biomimetic membranes. The relatively specific surface ~~are~~is of HAp also contributed to its better loading of the drug, while the effect differs depending on the type of carrier modification. The presence of curcuminoids in the hydroxyapatite changes the surface properties of the conjugate, which contributes to the low affinity of the nanocarrier to most of the tested membranes. Fluorouracil shows an accumulation in the structure of the lipids tested, but the use of hydroxyapatite as a carrier significantly reduces this type of interaction, while still, the nanocomposite interacts with biomimetic membranes.
Then, the nanocomposite loaded with a drug was tested *in vitro* on SKOV-3 and HepG2 cancer cells to check its cytotoxicity. It can be seen that the nanocomposite reveals the therapeutic effect towards both cancer cells confirming its potential to be applied in anticancer therapy. Depending on the cell type the nanocomposite uptake differs what shows the potential for the particular cancer types treatment.

Acknowledgements
Sunday J. Olusegun with No PPN/ULM/2020/1/00051/DEC/01, would like to thank the Polish National Agency for Academic Exchange (NAWA) for their support.

Funding
This work was supported by the Vietnam Academy of Science and Technology under grant No. CT0000.09/21-23.

References

Akter, J., Hossain, A., Takara, K., Islam, Z., 2019. Comparative Biochemistry and Physiology , Part C Antioxidant activity of di ff erent species and varieties of turmeric (Curcuma spp): Isolation of active compounds. Comp. Biochem. Physiol. Part C 215, 9–17.

Ayodele, O., Olusegun, S.J., Oluwasina, O.O., Okoronkwo, E.A., Beatriz, L., Olanipekun, E.O., Mohallem, N.D.S., Guimar, W.G., Gomes, F.D.M., Souza, G.D.O., Duarte, A., 2021. Experimental and theoretical studies of the adsorption of Cu and Ni ions from wastewater by hydroxyapatite derived from eggshells. Environ. Nanotechnology, Monit. Manag. 15.

Chao, I.-C., Wang, C.-M., Li, S.-P., Lin, L.-G., Ye, W.-C., Qing-Wen Zhang, 2018. Simultaneous Quantification of Three Curcuminoids and Three Volatile Components of Curcuma longa

Using Pressurized Liquid Extraction and High-Performance Liquid Chromatography. Molecules 23, 1568;

Chen, X., Zou, L.Q., Niu, J., Liu, W., Peng, S.F., Liu, C.M., 2015. The stability, sustained release and cellular antioxidant activity of curcumin nanoliposomes. Molecules 20, 14293–14311.

Dai, J., Wang, G., Ma, L., Wu, C., 2015. Study on the surface energies and dispersibility of graphene oxide and its derivatives. J. Mater. Sci. 50, 3895–3907.

Degot, P., Huber, V., Hofmann, E., Hahn, M., Touraud, D., Kunz, W., 2021. Solubilization and extraction of curcumin from Curcuma Longa using green , sustainable , and food-approved surfactant-free microemulsions. Food Chem. 336, 127660.

Ferreira-Ermita, D.A.C., Valente, F.L., Carlo-Reis, E.C., Araújo, F.R., Ribeiro, I.M., Cintra, C.C.V., Borges, A.P.B., 2020. Characterization and in vivo biocompatibility analysis of synthetic hydroxyapatite compounds associated with magnetite nanoparticles for a drug delivery system in osteomyelitis treatment. Results Mater. 5.

Gheisari, H., Karamian, E., Abdellahi, M., 2015. A novel hydroxyapatite -Hardystonite nanocomposite ceramic. Ceram. Int. 41, 5967–5975.

Grocholewicz, K., Matkowska-Cichocka, G., Makowiecki, P., Droździk, A., Ey-Chmielewska, H., Dziewulska, A., Tomasik, M., Trybek, G., Janiszewska-Olszowska, J., 2020. Effect of nano-hydroxyapatite and ozone on approximal initial caries: a randomized clinical trial. Sci. Rep. 10, 1–8.

Gupta, K.K., Pal, N., Mishra, P.K., Srivastava, P., Mohanty, S., Maiti, P., 2014. 5-Florouracil-loaded poly(lactic acid)-poly(caprolactone) hybrid scaffold: Potential chemotherapeutic implant. J. Biomed. Mater. Res. - Part A 102, 2600–2612.

Hadi, S., Artanti, A.N., Rinanto, Y., Wahyuni, D.S.C., 2018. Curcuminoid content of Curcuma longa L. and Curcuma xanthorrhiza rhizome based on drying method with NMR and HPLC-UVD. Mater. Sci. Eng. 567, 7–12.

Ismail, E.H., Sabry, D.Y., Mahdy, H., Khalil, M.M.H., 2014. Synthesis and Characterization of some Ternary Metal Complexes of Curcumin with 1,10-phenanthroline and their Anticancer Applications. J. Sci. Res. 6, 509–519.

Jin, J., Zuo, G., Xiong, G., Luo, H., Li, Q., Ma, C., Li, D., Gu, F., Ma, Y., Wan, Y., 2014. The inhibition of lamellar hydroxyapatite and lamellar magnetic hydroxyapatite on the migration and adhesion of breast cancer cells. J. Mater. Sci. Mater. Med. 25, 1025–1031.

Jin, L., Liu, Q., Sun, Z., Ni, X., Wei, M., 2010. Preparation of 5-fluorouracil/β-cyclodextrin complex intercalated in layered double hydroxide and the controlled drug release properties. Ind. Eng. Chem. Res. 49, 11176–11181.

Khan, S., Imran, M., Tahir, T., Wadood, S., Shah, A., Sohail, M., Malik, A., Das, S., Ei, H., Adam, A., Hussain, Z., 2018. Curcumin based nanomedicines as e ffi cient nanoplatform for treatment of cancer : New developments in reversing cancer drug resistance, rapid internalization, and improved anticancer efficacy. Trends Food Sci. Technol. 80, 8–22.

Lee, D., Wufuer, M., Kim, I., Choi, T.H., Kim, B.J., Jung, H.G., Jeon, B., Lee, G., Jeon, O.H., Chang, H., Yoon, D.S., 2021. Sequential dual-drug delivery of BMP-2 and alendronate from hydroxyapatite-collagen scaffolds for enhanced bone regeneration. Sci. Rep. 11, 1–10.

Lee, J.W., Kim, S.W., Cho, Y.L., Jeong, H.Y., Song, Y. Il, Suh, S.J., 2016. Dispersion stabilities of multi-layer graphene-coated copper prepared by electrical wire-explosion method. J. Nanosci. Nanotechnol. 16, 11286–11291.

Li, R., Xiang, C., Zhang, X., An Guo, D.-, Ye, M., 2010. Chemical Analysis of the Chinese Herbal Medicine Turmeric (Curcuma longa L.). Curr. Pharm. Anal. 6, 256–268.

Lili, Z., Hongfei, Z., Shoukat, S., Xiaochen, Z., Bolin, Z., 2017. Screening lactic acid bacteria strains with ability to bind di-n-butyl phthalate via Turbiscan technique. Antonie van Leeuwenhoek, Int. J. Gen. Mol. Microbiol. 110, 759–769.

Mujahid, M., Sarfraz, S., Amin, S., 2015. On the formation of hydroxyapatite nano crystals prepared using cationic surfactant. Mater. Res. 18, 468–472.

Mukerjee, A., Vishwanatha, J.K., 2009. Formulation , Characterization and Evaluation of Curcumin-loaded PLGA Nanospheres for Cancer Therapy. Anticancer Res. 3876, 3867–3875.

Naahidi, S., Jafari, M., Edalat, F., Raymond, K., Khademhosseini, A., Chen, P., 2013. Biocompatibility of engineered nanoparticles for drug delivery. J. Control. Release 166, 182–194.

Nguyen, P.T., Nguyen, X.T., Nguyen, T. Van, Nguyen, T.T., Vu, T.Q., Nguyen, H.T., Pham, N.T., Thi Dinh, T.M., 2020. Treatment of Cd2+ and Cu2+ Ions Using Modified Apatite Ore. J. Chem. 2020.

Núñez, D., Serrano, J.A., Mancisidor, A., Elgueta, E., Varaprasad, K., Oyarzún, P., Cáceres, R., Ide, W., Rivas, B.L., 2019. Heavy metal removal from aqueous systems using hydroxyapatite nanocrystals derived from clam shells. RSC Adv. 9, 22883–22890.

Nurjanah, N., Saepudina, E., 2020. Curcumin Isolation, Synthesis and Characterization of Curcumin Isoxazole Derivative Compound. AIP Conf. Proc. 2168, 020065.

Pan, Y., Ju, R., Cao, X., Pei, H., Zheng, T., Wang, W., 2020. Optimization extraction and purification of biological activity curcumin from Curcuma longa L by high-performance counter-current chromatography. J. Sep. Sci. 43, 1586–1592.

Qi, X., Dong, Y., Wang, H., Wang, C., Li, F., 2017. Application of Turbiscan in the homoaggregation and heteroaggregation of copper nanoparticles. Colloids Surfaces A Physicochem. Eng. Asp. 535, 96–104.

Ram Prasad, S., Jayakrishnan, A., Sampath Kumar, T.S., 2019. Hydroxyapatite-poly(vinyl alcohol) core-shell nanoparticles for dual delivery of methotrexate and gemcitabine for bone cancer treatment. J. Drug Deliv. Sci. Technol. 51, 629–638.

Ranjha, M.M.A.N., Shafique, B., Rehman, A., Mehmood, A., Ali, A., Zahra, S.M., Roobab, U., Singh, A., Ibrahim, S.A., Siddiqui, S.A., 2022. Biocompatible Nanomaterials in Food Science, Technology, and Nutrient Drug Delivery: Recent Developments and Applications. Front. Nutr. 8, 1–15.

Ren, Y., Zheng, Jiaxing, Xu, Z., Zhang, Y., Zheng, Jianping, 2018. Application of Turbiscan LAB to study the influence of lignite on the static stability of PCLWS. Fuel 214, 446–456.

Shaban, M., Abukhadra, M.R., Mohamed, A.S., Shahien, M.G., Ibrahim, S.S., 2018. Synthesis of Mesoporous Graphite Functionalized by Nitrogen for Efficient Removal of Safranin Dye Utilizing Rice Husk Ash; Equilibrium Studies and Response Surface Optimization. J. Inorg. Organomet. Polym. Mater. 28, 279–294.

Slosarczyka, A., Paszkiewicza, Z., Paluszkiewicz, C., 2005. FTIR and XRD evaluation of carbonated hydroxyapatite powders synthesized by wet methods. J. Mol. Struct. 744–747 747, 657–661.

Song, J., Cui, N., Mao, X., Huang, Q., Lee, E.S., Jiang, H., 2022. Sorption Studies of Tetracycline Antibiotics on Hydroxyapatite (001) Surface—A First-Principles Insight. Materials (Basel). 15.

Sun, W., Fan, J., Wang, S., Kang, Y., Du, J., Peng, X., 2018. Biodegradable Drug-Loaded Hydroxyapatite Nanotherapeutic Agent for Targeted Drug Release in Tumors. ACS Appl. Mater. Interfaces 10, 7832–7840.

Xu, L. lu, Shang, Z. peng, Lu, Y. ying, Li, P., Sun, L., Guo, Q. lei, Bo, T., Le, Z. yong, Bai, Z. li, Zhang, X. li, Qiao, X., Ye, M., 2020. Analysis of curcuminoids and volatile components in 160 batches of turmeric samples in China by high-performance liquid chromatography and gas chromatography mass spectrometry. J. Pharm. Biomed. Anal. 188, 1–7.

Zhao, X., Ng, S., Heng, B.C., Guo, J., Ma, L., Tan, T.T.Y., Ng, K.W., Loo, S.C.J., 2013. Cytotoxicity of hydroxyapatite nanoparticles is shape and cell dependent. Arch. Toxicol. 87, 1037–1052.

Zhong, Z., Woo, K., Kim, I., Hwang, H., Kwon, S., Choi, Y.M., Lee, Y., Lee, T.M., Kim, K., Moon, J., 2016. Roll-to-roll-compatible, flexible, transparent electrodes based on self-nanoembedded Cu nanowires using intense pulsed light irradiation. Nanoscale 8, 8995–9003.

Zhou, H., Lee, J., 2011. Nanoscale hydroxyapatite particles for bone tissue engineering. Acta

Biomater. 7, 2769–2781.

Zuo, G., Wan, Y., Meng, X., Zhao, Q., Ren, K., Jia, S., Wang, J., 2011. Synthesis and characterization of a lamellar hydroxyapatite/DNA nanohybrid. Mater. Chem. Phys. 126, 470–475.

[i] Peetla Ch., Jin S., Weimer J., Elegbede A., Labhasetwar V., Biomechanics and Thermodynamics of Nanoparticle Interactions with Plasma and Endosomal Membrane Lipids in Cellular Uptake and Endosomal Escape Langmuir 2014 30 7522-7532

[ii] Elderdfi M., Sikorski A. F., Langmuir-monolayer methodologies for characterizing protein-lipid interactions, *Chemistry and Physics of Lipids*, **2018** 212 61-72

[iii] Nieciecka D., Rękorajska A., Cichy D., Końska P., Żuk M., Krysiński P., Synthesis and Characterization of Magnetic Drug Carriers Modified with Tb3+ Ions, Nanomaterials 2022, 12, 795

[v] Jurak M., Szafran K., Cea P., Analysis of Molecular Interactions between Components in Phospholipid-Immunosuppressant-Antioxidant Mixed Langmuir Films Langmuir 2021 37 5601-5616

[vi] Davies, J. T.; Rideal, E. K. Interfacial Phenomena, 2nd ed.; Academic Press: New York, 1963.

[vii] Nieciecka, D.; Celej, J.; Żuk, M.; Majkowska-Pilip, A.; Żelechowska-Matysiak, K.; Lis, A.; Osial, M. Hybrid System for Local Drug Delivery and Magnetic Hyperthermia Based on SPIONs Loaded with Doxorubicin and Epirubicin. Pharm. 2021, 13.